Differential involvement of oriens/pyramidale interneurones in hippocampal network oscillations *in vitro*

Tengis Gloveli[1,2], Tamar Dugladze[1,2], Sikha Saha[1], Hannah Monyer[3], Uwe Heinemann[2], Roger D. Traub[4], Miles A. Whittington[1] and the late Eberhard H. Buhl[1]

[1]*School of Biomedical Sciences, Worsley Building, University of Leeds, Leeds LS2 9JT, UK*
[2]*Johannes-Müller-Institute of Physiology at the charité, Humboldt University Berlin, Tucholskystr. 2, 10117 Berlin, Germany*
[3]*University Hospital Neurology, Department of Clinical Neurobiology Im Neuenheimerfeld 364, Heidelberg D-69120, Germany*
[4]*Department of Physiology and Pharmacology, SUNY Health Science Center, Brooklyn, NY 11203, USA*

Using whole-cell patch-clamp recordings in conjunction with *post hoc* anatomy we investigated the physiological properties of hippocampal stratum oriens and stratum pyramidale inhibitory interneurones, before and following the induction of pharmacologically evoked gamma frequency network oscillations. Prior to kainate-induced transient epochs of gamma activity, two distinct classes of oriens interneurones, oriens lacunosum-moleculare (O-LM) and trilaminar cells, showed prominent differences in their membrane and firing properties, as well as in the amplitude and kinetics of their excitatory postsynaptic events. In the active network both types of neurone received a phasic barrage of gamma frequency excitatory inputs but, due to their differential functional integration, showed clear differences in their output patterns. While O-LM cells fired intermittently at theta frequency, trilaminar interneurones discharged on every gamma cycle and showed a propensity to fire spike doublets. Two other classes of fast spiking interneurones, perisomatic targeting basket and bistratified cells, in the active network discharged predominantly single action potentials on every gamma cycle. Thus, within a locally excited network, O-LM cells are likely to provide a theta-frequency patterned output to distal dendritic segments, whereas basket and bistratified cells are involved in the generation of locally synchronous gamma band oscillations. The anatomy and output profile of trilaminar cells suggest they are involved in the projection of locally generated gamma rhythms to distal sites. Therefore a division of labour appears to exist whereby different frequencies and spatiotemporal properties of hippocampal rhythms are mediated by different interneurone subtypes.

(Resubmitted 31 July 2004; accepted after revision 11 October 2004; first published online 14 October 2004)
Corresponding author T. Gloveli: Johannes-Müller-Institut für Physiologie, Charité Universitätsmedizin Berlin, Tucholskystr. 2, 10117 Berlin, Germany. Email: tengis.gloveli@charite.de

Synchronous gamma-frequency oscillations (30–80 Hz) represent a temporally coherent activity and are thought to be important in cortical information processing (Gray & Singer, 1989; Jones & Barth, 1997; Ritz & Sejnowski, 1997; Fries *et al.* 2001). One of their putative roles may be the synchronization of groups of spatially segregated cortical neurones at sites that can be many millimetres apart (Gray *et al.* 1989). Synchronous activity is ideally suited to provide a mechanism for the functional 'binding' of sensory features. Gamma frequency oscillations have been observed in a variety of brain structures (Singer & Gray, 1995), amongst them the hippocampus, which has a key role in memory formation (Morris *et al.* 1982; Zola-Morgan & Squire, 1993), and shows oscillatory activity in the theta/gamma frequency band during specific behavioural states (Buzsaki *et al.* 1983; Soltesz & Deschenes, 1993; Sik *et al.* 1995; Singer & Gray, 1995; Penttonen *et al.* 1998). There is compelling evidence that hippocampal interneurones have a pivotal role in driving inhibition-based rhythms, such as gamma and theta frequency network oscillations (Whittington *et al.* 1995; Fisahn *et al.* 1998; Hormuzdi *et al.* 2001; Gillies *et al.* 2002; Klausberger *et al.* 2003, 2004).

Interneurones can be broadly classified into several classes on the basis of different criteria, such as action potential firing properties, somato-dendritic architecture and axonal ramification pattern, neurochemical content, voltage and ligand-gated conductances as well as plastic changes in excitatory synaptic transmission (for reviews see Freund & Buzsaki, 1996; McBain & Fisahn, 2001;

 DOI: 10.1113/jphysiol.2004.073007

Maccaferri & Lacaille, 2003). One of the classification schemes is based on the axonal ramification patterns of interneurones and, in particular, the innervation of spatially segregated domains on the somato-dendritic surface of principal cells. Thus hippocampal interneurones can be divided into perisomatic targeting interneurones, such as basket and axo-axonic cells, and dendrite targeting cells, such as oriens lacunosum-moleculare (O-LM), bistratified and trilaminar interneurones (Buhl *et al.* 1994; Freund & Buzsaki, 1996). Within this broad classification scheme further subdivision is possible based on the proximo-distal segregation of efferent target domains (Maccaferri *et al.* 2000). Although it is reasonable to assume that the anatomical heterogeneity of hippocampal interneurones is reflected in their functional diversity, in particular during different forms of network activity, there are few studies which have attempted a correlation of structure and function. In particular, the way in which oscillatory input affects the activity of individual interneurones in the active network remains to be clarified.

Whole-cell patch-clamp recordings using infrared differential contrast videomicroscopy (Dodt & Zieglgansberger, 1990, 1994) have greatly expanded our understanding of interneurone function. However, this approach has been hampered due to the difficulty of generating physiologically relevant population activity, such as network oscillations in submerged conditions. In the present study we employ brief pressure ejections of kainate to generate oscillatory network activity in submerged slices. Using a technical modification of a pharmacological protocol which, in mechanistic terms, is reasonably well understood (Traub *et al.* 2000; Hormuzdi *et al.* 2001), we were able, for the first time, to record from visually identified interneurones during gamma frequency network oscillation. By correlating the physiological properties of distinct types of anatomically identified hippocampal interneurones we were able to demonstrate that these anatomically heterogeneous cell classes show differences in some of their biophysical properties, synaptic mechanisms and firing patterns. These different properties of interneurones, in turn, determine their differential involvement in the generation of hippocampal oscillatory network activity. In addition, we also address the unresolved issue as to how the hippocampal network can generate 'nested' rhythms concurrently occurring in the theta and gamma frequency bands.

Methods

Slice preparation

Brains were taken from C57BL6 mice (P18–25), anaesthetized with a lethal dose of inhaled isoflurane, immediately followed by an I.M. injection of ketamine ($100\ mg\ kg^{-1}$) and xylazine ($10\ mg\ kg^{-1}$) in accordance with the UK Animals (Scientific Procedures) Act 1986. Horizontal combined entorhinal cortex–hippocampal slices ($450\ \mu m$ thick) were prepared using a tissue slicer (Leica VT 1000S, Nussloch, Germany).

Perisomatic interneurones were studied using transgenic mice that expressed enhanced fluorescent protein under the control of the parvalbumin promoter. Transgenic mice were generated using bacterial artificial chromosome techniques, as described in detail elsewhere (Meyer *et al.* 2002). Slices were incubated at room temperature for at least 1 h in a holding chamber and then transferred to the recording chamber. The solution used during incubation and recording contained (mM): NaCl, 126; KCl, 3; NaH_2PO_4, 1.25; $CaCl_2$, 2; $MgSO_4$, 2; $NaHCO_3$, 24; glucose, 10, saturated with 95% O_2 and 5% CO_2.

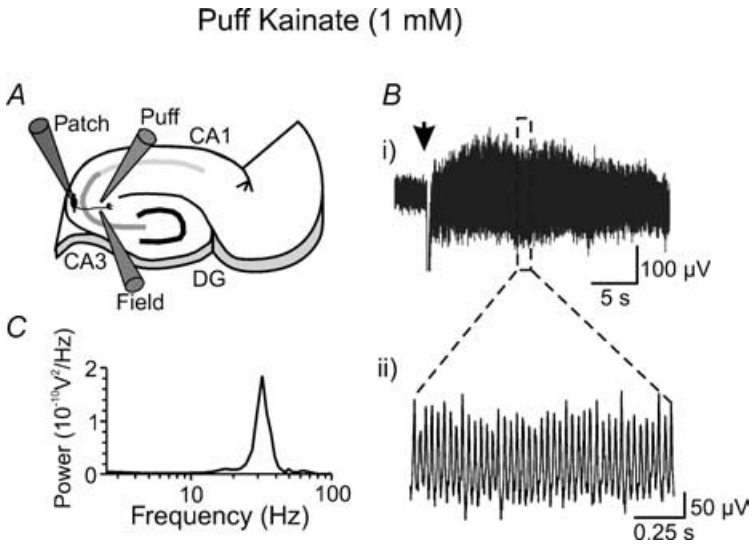

Figure 1. Properties of gamma frequency network oscillations evoked in submerged slices
A, schematic illustration showing the placement of the injecting (Puff) and recording pipettes within the hippocampal area CA3. Kainate was pressure ejected onto the surface of stratum radiatum. Concomitant with extracellular field potential recordings in stratum radiatum close to the application site (Field), whole-cell patch-clamp recordings were obtained from stratum oriens/pyramidale interneurones (Patch). CA1, area CA1; CA3, area CA3; DG, dentate gyrus. *Bi*, representative extracellular recording following puff-applied kainate (1 mM, application indicated by the arrow) shows a transient episode of gamma frequency oscillatory activity. The oscillatory activity occurs upon recovery from the transient small negative DC shift (truncated for clarity). *ii*, character of the oscillations in an expended time scale. *C*, the mean power spectrum shows a distinct peak at ~32 Hz ($n = 8$).

Extracellular field recordings

Experiments were performed at 29°C in a submerged-type chamber. ACSF in the submerged chamber was maintained at a low level and the rate of superfussion with the ACSF was 3–4 ml min^{-1}. The ejecting and recording electrodes were maintained in close proximity (typically < 0.2 mm) so as to get prominent field oscillations. Field potential recordings and pressure application of kainate (1 mM, 60 p.s.i., duration 10–60 ms) were done in the stratum radiatum of area CA3 using patch pipettes. Ejected volume was generally correlated with oscillatory peak power and duration, whereas the peak frequency remained constant for any given slice. Field potentials were recorded with an Axoclamp 2B amplifier (Axon Instruments, Union City, CA, USA). Data were digitized with an ITC-16 A/D board (Instrutech Corp., Port Washington, NY, USA) and further analysed using Axograph (Axon Instruments) and KaleidaGraph (Synergy Software, Reading, PA, USA) software. Oscillatory peak frequency was determined by averaging several consecutive Fourier transforms, contained within a 2–30 s epoch. Power in the gamma frequency band was calculated by integration of power spectra between 20 and 80 Hz. Auto- and cross-correlations were calculated over a 2 s epoch. Student's *t* test was used for

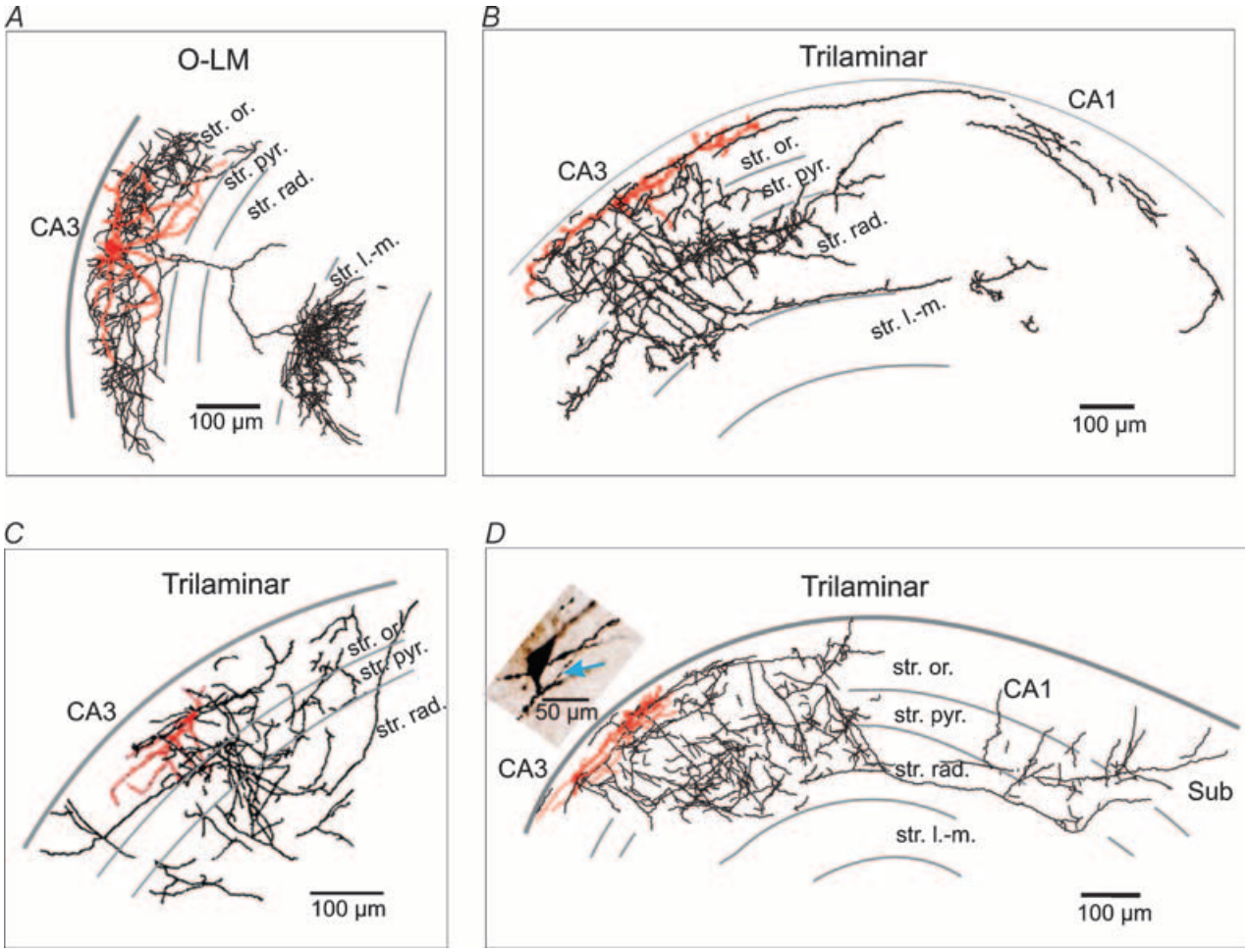

Figure 2. Morphological characterization of O-LM and trilaminar interneurones in stratum oriens
Reconstructions of representative biocytin-filled O-LM (*A*) and three trilaminar (*B–D*) cells. The soma and dendrites are drawn in red, whereas the axons are in black. The horizontal dendritic branches from both interneurone types are restricted to the stratum oriens. The O-LM cell had an axon that crossed the pyramidal cell layer and extensively arborized in the stratum lacunosum-moleculare of the area CA3, while the axons from the trilaminar cell arborized in three layers (str. oriens, pyramidale and radiatum). Axon collaterals of the trilaminar cell in *B* extend horizontally (~1.3 mm) throughout the CA1 area of the hippocampus, whereas a ~1.5 mm long axonal branch of another trilaminar cell in *D* traverses the entire extent of the CA1 are a and reaches the subiculum. Note the axon initial segment (arrow) in the trilaminar interneurone (*D*, inset). Hippocampal layers are depicted schematically. CA3, CA3 area; CA1, CA1 area; Sub, subiculum; str. or., stratum oriens; str. pyr., stratum pyramidale; str. rad., stratum radiatum; str. l.-m., stratum lacunosum-moleculare.

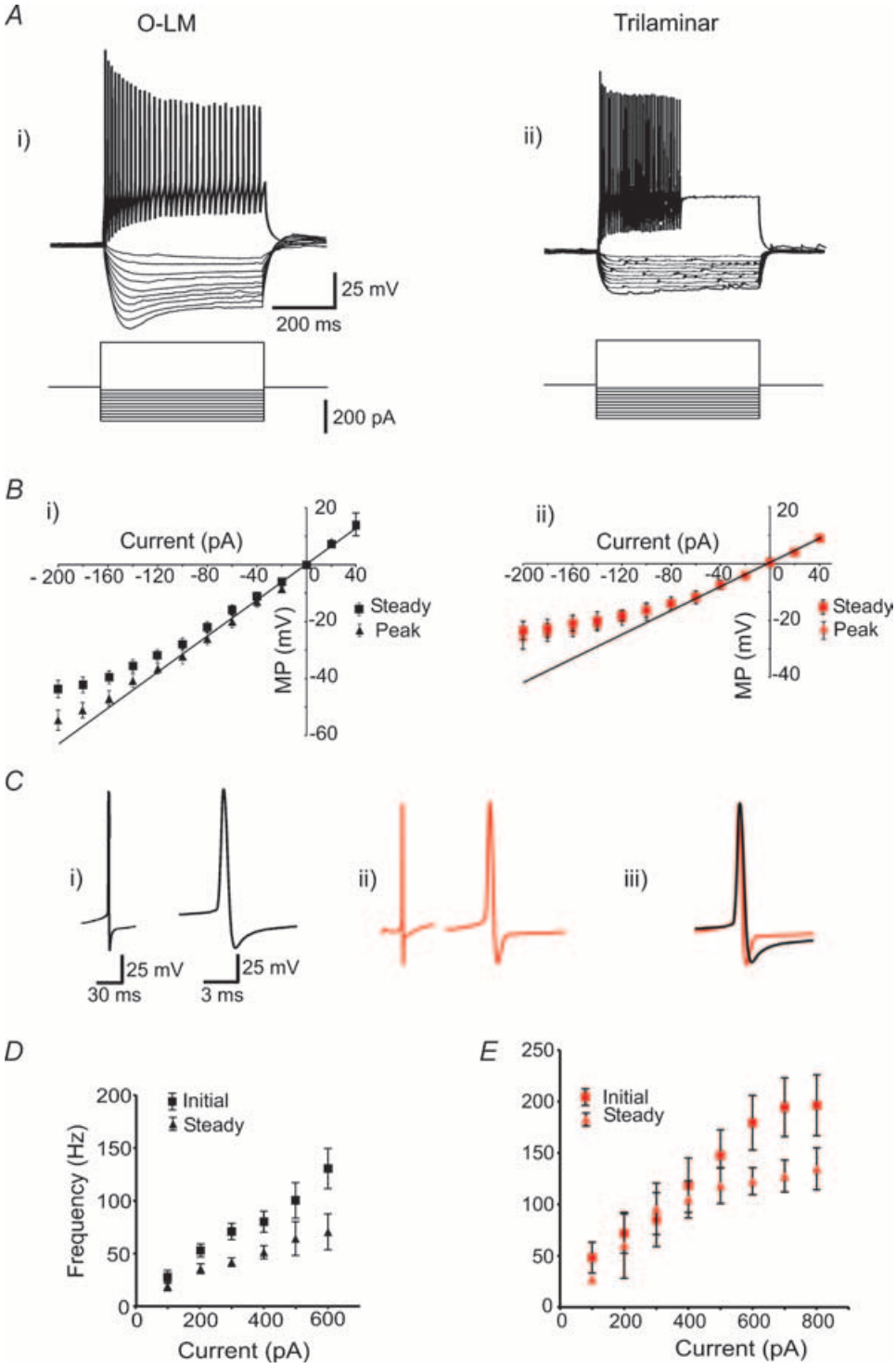

Figure 3. Intrinsic membrane properties and the firing patterns of O-LM and trilaminar interneurones
A, the firing patterns and the intrinsic membrane properties of the O-LM (*i*, upper traces) and trilaminar (*ii*, upper traces) interneurones during 500 ms-long depolarizing (300 pA for both O-LM and trilaminar cells) and hyperpolarizing intrasomatic current injection (of –200 pA to –20 pA in 20-pA increments for both cell types; lower traces, V_m –70 mV). O-LM (*i*) but not trilaminar (*ii*) cell shows the clear 'sag' at stronger hyperpolarizing current injection (sag ratio at –200 pA was 0.73). Note sudden periods of silence in trilaminar cells during a prolonged current step and typical suppression of action potential amplitude in O-LM cells (which normally no longer discharged at > 600 pA depolarizing current injection, see *D*). *B*, voltage–current relationship for O-LM (*i*, black, $n = 8$) and trilaminar (*ii*, red, $n = 6$) cells. ■, steady state voltages; ▲, peak responses, most of which overlap in trilaminar cells. Note clear differences between steady state and peak responses in O-LM cells at more

Table 1. Intrinsic and firing properties of hippocampal oriens/pyramidale interneurones and pyramidal cells

Cell type	O-LM ($n = 15$)	Trilaminar ($n = 8$)	Basket ($n = 6$)	Bistratified ($n = 3$)	Pyramid ($n = 9$)
Resting membrane potential (mV)	-60.0 ± 3.1	-61.2 ± 4.6	-58.5 ± 2.8	-61.3 ± 5.2	-65.8 ± 6.5
Input resistance (MΩ)	315.1 ± 41.6	167.3 ± 20.9*	122.9 ± 10.9*	138.8 ± 8.1*	160.1 ± 13.6
Membrane time constant (ms)	33.3 ± 1.4	16.9 ± 3.1*	11.2 ± 1.2*	18.8 ± 1.6*	37.2 ± 3.6
Single action potential					
Half-duration (ms)	0.84 ± 0.04	0.57 ± 0.01*	0.54 ± 0.04*	0.63 ± 0.04*	1.18 ± 0.08
AHP decay time constant (ms)	4.58 ± 0.53	0.49 ± 0.07*	0.82 ± 0.10*	1.20 ± 0.36*	7.71 ± 0.95
AHP half-duration (ms)	5.15 ± 1.55	0.82 ± 0.13*	0.98 ± 0.10*	1.60 ± 0.51*	8.33 ± 1.56
Repetitive firing					
Spikes/nA (within 200 ms)	36.4 ± 4.1	50.3 ± 4.4*	47.2 ± 5.1	46.8 ± 7.1	27.0 ± 2.8
Kainate-evoked firing					
Spikes/gamma cycle	0.26 ± 0.04	1.82 ± 0.07*	1.28 ± 0.06*	1.04 ± 0.05*	0.18 ± 0.05
Frequency peak (Hz)	8.3 ± 2.1	32.1 ± 2.8*	33.6 ± 2.6*	35.0 ± 2.5*	3.5 ± 0.6
Peak power ($mV^2\ Hz^{-1}$)	1.9 ± 0.2	4.2 ± 0.3*	3.7 ± 0.3*	2.9 ± 0.5*	1.3 ± 0.4

Values are means ± S.E.M. *Significant differences in the values of fast spiking interneurones *versus* O-LM cells (*t* test). Repetitive firing parameters were measured within a shorter time interval (200 ms) because of sudden periods of silence in trilaminar cells during a prolonged (500 ms) current step.

statistical comparisons; differences were considered significant if $P < 0.05$. Average values are expressed as the mean ± S.E.M.

Whole-cell recordings

Concomitant with the extracellular field potential whole-cell patch-clamp recordings in current and voltage clamp mode were obtained from stratum oriens and pyramidale interneurones or pyramidal cells of area CA3 visualized by infrared differential interference contrast (DIC) videomicroscopy (Zeiss Axioscope microscope, Hamamatsu CCD camera, Luigs & Neumann Infrapatch set-up). Whole-cell recording pipettes (3–5 MΩ) were filled with a solution containing (mM): potassium gluconate, 135; KCl, 5; ATP-Mg, 2; GTP-Na, 0.3; Hepes, 10; plus biocytin, 0.5% (pH 7.3 and 280 mosmol l^{-1}). An Axopatch 1D amplifier (Axon Instruments) was used for current- and voltage-clamp recordings. The holding potentials were –60 mV and –70 mV for current- and voltage-clamp recordings, respectively, unless indicated otherwise. The seal resistance before establishing whole-cell mode was ≥ 2 GΩ. The series resistance was monitored repeatedly during the experiment by measuring the amplitude of the capacitive current in response to a –10 mV pulse. Series resistance (range 12–18 MΩ) was not significantly different between different interneurone types (14.2 ± 0.9 MΩ ($n = 15$), 15.1 ± 0.8 MΩ ($n = 8$), 13.4 ± 1.2 MΩ ($n = 6$) and 15.3 ± 1.4 MΩ ($n = 3$) in O-LM, trilaminar, basket and bistratified cells, respectively). Voltage measurements were not corrected for the potassium gluconate junction potential.

The intrinsic properties of cells were measured in whole-cell current-clamp mode. The resting membrane potential was estimated during the absence of a holding current. The input resistance and membrane time constant were estimated from voltage responses to current injection (500 ms; ± 100 pA, at 10 pA increments). The input resistance was determined from the slope of the steady state responses in a linear region around, and including, the origin. The membrane time constant was obtained from the slowest time constant of exponential fits to voltage transients in the same linear region of the *I–V* plot (see Spruston *et al.* 1997). 'Sag' was quantified by the ratio of the steady state voltage to the peak voltage in response to current injections (–200 pA, 500 ms). As recorded cells did not fire action potentials at rest, the analysis of the amplitude and duration of action potentials as well as decay time constant and half-duration of afterhyperpolarization (AHP) were performed on first action potential discharges elicited by stepwise increased constant depolarizing current injection, causing small (∼5 mV) graded voltage changes. The recorded

hyperpolarizing level. The lines shown are linear regressions through the steady state points between –40 pA and +40 pA in O-LM (*i*) and –60 pA and +40 pA in trilaminar cells (*ii*). *C*, action potentials in O-LM cells (*i*) are characterized by their longer duration and are followed by a longer AHPs as those in trilaminar cells (*ii*) that are more clearly visible in superimposed traces normalized for amplitude (*iii*, black, O-LM cell; red, trilaminar cell). *D* and *E*, initial (between 1st and 2nd action potentials) (■) and steady state (between last and penultimate action potentials) (▲) firing frequencies of trains of APs elicited in O-LM (*D*) and trilaminar (*E*) cells ($n = 6$ for each cell types) by depolarizing current injection against the amplitude of the pulses. Error bars indicate S.E.M.

interneurones typically showed rapid-onset, deep spike AHP which decayed rapidly and monophasically. The duration of action potentials was measured at half-amplitude. The accommodation parameters were measured on discharges elicited by application of 500 ms depolarizing current pulses. Repetitive firing in response to depolarizing current injection (500 ms) was evaluated by measuring the number of spikes *versus* the amplitude of injected current (up to 600 pA). The action potential discharge frequency was measured between the first two spikes (initial) and at the end of firing (steady-state) during a depolarizing current injection (500 ms) at all stimulation intensities tested.

The spontaneous excitatory postsynaptic currents (EPSCs) and potentials (EPSPs) as well as kainate-evoked EPSCs were measured at the reversal potential for $GABA_A$ receptor-mediated events (around –70 mV). The threshold of spontaneous and evoked EPSCs was determined from their absolute amplitude. Because of the very high frequency of kainate-evoked individual events of compound EPCSs, these events were carefully selected after visual inspection of recorded traces in order to discard supposed bi- or multiquantal events. Particularly, single events typically detectable at the rising part of kainate-evoked compound EPSCs, which due to their distinct time course allowed us to measure their 10–90% rise time and decay time constant, were individually selected. The individual events (40 events from each cell) were aligned for averaging and calculating kinetic parameters of EPSCs. Postsynaptic events as well as the inter-event interval of compound EPSCs (from *ca* 600 events) were further analysed with Mini Analysis Program (Synaptosoft, Decatur, GA, USA).

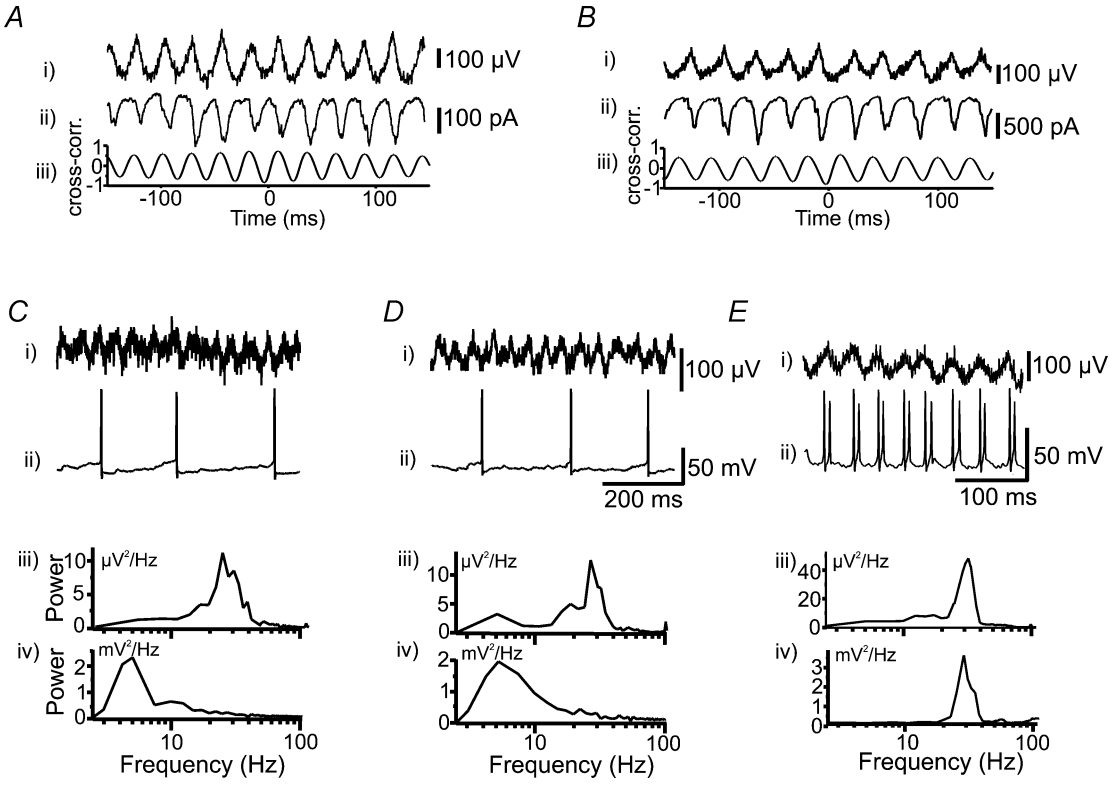

Figure 4. Properties of O-LM and trilaminar cells during kainate induced network oscillations
A and *B*, typical example of extracellular field (*i*) and concomitant voltage clamp recordings (*ii*) in an O-LM (*A*) and trilaminar (*B*) cells following induction of oscillatory activity. At a holding potential of –70 mV, rhythmic excitatory postsynaptic currents (EPSCs) are apparent in both cell types, but were markedly larger in trilaminar than in O-LM cells. Note inflections in the rising phase of excitatory events indicating their compound nature. Cross-correlations of the extracellular and voltage clamp traces (*iii*) show that interneurone postsynaptic currents in both cell types are phase related to the extracellular field. *C–E*, current clamp recordings at –60 mV (*Cii*) and –50 mV (*Dii*) from O-LM and at –60 mV from trilaminar (*Eii*) cells show firing patterns of these cells during gamma frequency network oscillations. Note similar firing pattern of an O-LM cell at rest and at more depolarizing membrane potential close to firing threshold. During oscillatory activity O-LM cells fire sporadically (*Cii* and *Dii*), whereas trilaminar cells (*Eii*) generate regular action potential doublets on every cycle. *Ciii–iv*, *Diii–iv* and *Eiii–iv*, power spectra illustrating oscillatory activity at the theta (*Civ*, *Div*) and gamma frequency (*Eiv*) range in O-LM and trilaminar interneurones, respectively, during the field gamma frequency oscillations (*Ciii*; *Diii* and *Eiii*).

Signals were filtered at 5 kHz (whole-cell recording) or 0.002–1 kHz (extracellular field potential recording) with an external 8-pole Bessel filter (Applegarth Electronics, Oxford, UK) and digitized at 10 kHz using an ITC-16 A/D board (Instrutech). EPSC and AHP kinetics (decay time constant, half-duration) were studied using Mini Analysis Program. The Kolmogorov-Smirnov statistical test was used to compare two different cumulative distributions with $P < 10^{-4}$ reaching statistical significance.

Anatomical identification of interneurones

Slices with a biocytin-filled interneurone were sandwiched between two Millipore filters to avoid deformation and fixed in 0.1 mM phosphate buffer (pH 7.4) containing 4% paraformaldehyde, 0.05% glutaraldehyde and 15% saturated picric acid at 4°C for 24–48 h. Following gelatine embedding, 75 μm sections of the slices were prepared. The filled neurones were visualized by incubating sections in avidin–biotin conjugated horseradish peroxidase (ABC, Vector Laboratories, Ltd, UK) and reacting them with diaminobenzidine and hydrogen peroxide. Sections were then intensified in 0.5% OsO_4, dehydrated and embedded into epoxy resin (Durcupan, Sigma) on glass slides. Subsequently, the cells were reconstructed with the aid of a camera lucida or a Neurolucida 3D reconstruction system (MicroBrightField, Inc., Williston, VT, USA).

Results

Network gamma oscillations in submerged slices

We employed a pharmacological gamma-induction protocol to study network oscillations in submerged slices. Pressure ejection of kainate (1 mM) onto stratum radiatum of the hippocampal CA3 area reliably and repeatedly induced a transient (8–40 s) period of network gamma frequency (γ) oscillations that could be detected with an extracellular field electrode located in close proximity to the ejection site ($n = 47$, Fig. 1*A* and *B*). The onset of the oscillation was preceded by a small (200–800 μV) and short (< 1 s) negative-going DC shift in the field recording (Fig. 1*B*). The power spectrum of the oscillatory activity shows a prominent peak in the gamma frequency range (Fig. 1*C*). The mean frequency of the γ oscillations was 32.8 ± 0.6 Hz ($n = 47$).

Morphological identification of oriens/pyramidale interneurones

Concomitant with extracellular field potential recordings whole-cell patch-clamp recordings were obtained from interneurones in stratum oriens/alveus of area CA3 of the hippocampus. Stratum oriens interneurones were morphologically diverse. Based on their somato-dendritic architecture and their axonal ramification pattern they could be classified into several groups (see also Maccaferri *et al.* 2000; for review see Freund & Buzsaki, 1996). For further detailed analysis, we selected two classes of *post hoc* anatomically identified horizontal cells, dendrite-targeting oriens lacunosum-moleculare (O-LM, $n = 15$) and trilaminar ($n = 8$) interneurones. These are clearly distinguishable as they establish spatially segregated postsynaptic target domains on distal *versus* proximal pyramidal dendrites and have characteristic electrophysiological properties. In addition bistratified ($n = 3$), and parvalbumin (PV)-positive perisomatic targeting

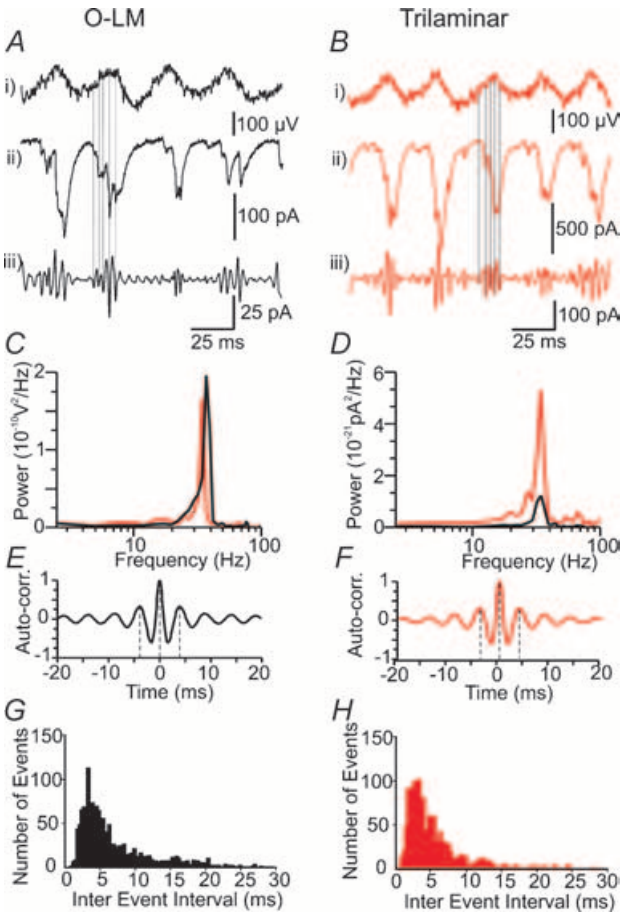

Figure 5. Compound interneuronal EPSCs contain a high-frequency oscillatory component
A and *B*, simultaneous field potential (*i*) and EPSC (*ii*) recordings from O-LM (*A*) and trilaminar (*B*) cells voltage clamped at –70 mV. In band pass filtered (200–500 Hz; *iii*) traces interneurones show a cycle-by-cycle waxing and waning of a high-frequency oscillatory component. *C* and *D*, corresponding mean power spectra of underlying gamma band activity from extracellular (*C*) and unfiltered patch clamp recording (*D*) for O-LM (black) and trilaminar (red) cells. *E* and *F*, auto-correlograms of band-pass filtered traces showing ripple-like activity in both O-LM (*E*) and trilaminar (*F*) cells, which is also apparent in corresponding histograms of inter-event intervals from unfiltered patch clamp recordings in both O-LM (*G*) and trilaminar (*H*) cells.

Table 2. Properties of EPSC/P in hippocampal oriens/pyramidale interneurones and pyramidal cells

Cell type	O-LM ($n = 8$)	Trilaminar ($n = 6$)	Basket ($n = 6$)	Bistratified ($n = 3$)	Pyramid ($n = 6$)
Spontaneous EPSP					
Amplitude (mV)	2.0 ± 0.1	2.9 ± 0.1*	2.4 ± 0.2	2.4 ± 0.2	1.7 ± 0.3
10–90% rise time (ms)	1.6 ± 0.4	0.8 ± 0.1*	1.2 ± 0.2	1.1 ± 0.1	3.8 ± 0.7
Decay time constant (ms)	5.9 ± 0.8	3.9 ± 0.2*	4.1 ± 0.5*	4.4 ± 0.2*	8.8 ± 1.6
Spontaneous EPSC					
Amplitude (pA)	37.5 ± 1.2	72.3 ± 4.4*	71.1 ± 7.2*	39.9 ± 5.3	37.9 ± 8.6
10–90% rise time (ms)	0.84 ± 0.10	0.48 ± 0.02*	0.54 ± 0.02*	0.56 ± 0.05*	1.45 ± 0.13
Decay time constant (ms)	2.58 ± 0.09	1.65 ± 0.09*	1.62 ± 0.25*	1.38 ± 0.17*	4.62 ± 0.64
Kainate-evoked individual EPSC					
Amplitude (pA)	54.3 ± 1.7	150.2 ± 8.9*	115.2 ± 18.7*	94.1 ± 4.3*	42.3 ± 9.1
10–90% rise time (ms)	0.84 ± 0.09	0.53 ± 0.05*	0.60 ± 0.04*	0.60 ± 0.06*	1.50 ± 0.15
Decay time constant (ms)	2.52 ± 0.20	1.40 ± 0.23*	1.50 ± 0.15*	1.43 ± 0.02*	4.68 ± 0.83
Inter-event interval (ms)	3.30 ± 0.15	3.22 ± 0.20	4.22 ± 0.21*	4.59 ± 0.21*	9.7 ± 1.9
Kainate-evoked compound EPSC					
Frequency peak (Hz)	32.9 ± 2.1	31.4 ± 2.2	33.3 ± 3.1	35.1 ± 3.3	31.3 ± 3.4
Peak power (nA^2Hz^{-1})	0.011 ± 0.01	0.046 ± 0.02*	0.041 ± 0.02*	0.035 ± 0.02*	0.008 ± 0.02

Values are means ± S.E.M. *Significant differences in the values of fast spiking interneurones *versus* O-LM cells (*t* test).

interneurones ($n = 6$) in stratum oriens/pyramidale as well as CA3 pyramidal cells ($n = 9$) were studied for comparison. Having largely similar physiological and morphological (basket-like) features, PV-positive cells were grouped together and classified as perisomatic interneurones. About one-third of recorded interneurones could not be completely reconstructed, either because of their proximity to the slice surface or because of the incomplete labelling. We excluded these cells from our study.

All recorded and biocytin-labelled O-LM interneurones displayed a previously described horizontal organization of dendritic tree and axonal termination in the stratum oriens and lacunosum-moleculare (Fig. 2*A*, see also Ali & Thomson, 1998; Maccaferri *et al.* 2000), coaligned with the distal apical dendrites of the pyramidal cells. The trilaminar cells have the similar horizontally distributed dendrites in stratum oriens, but are clearly different from O-LM cells in respect of axonal arborization (Fig. 2*B–D*) and exibit clearly different physiological features. In contrast to the O-LM cells, the trilaminar interneurone had axon collaterals in strata oriens, pyramidale and radiatum (see also, Sik *et al.* 1995) which extended a long distance transversally in the area CA1/subicular direction (Fig. 2*B* and *D*).

Electrophysiological characterization of morphologically identified horizontal stratum oriens interneurones

There were no significant differences in the resting membrane potentials of O-LM and trilaminar interneurones. O-LM interneurones had a significantly higher input resistance and slower membrane time constant than trilaminar cells (Table 1). A consistent electrophysiological feature of O-LM cells contrasting the trilaminar and all other studied interneurones was the 'sag' in response to hyperpolarizing current injection (Fig. 3*A* and *B*, see also Lacaille & Williams, 1990; Sik *et al.* 1995; Maccaferri & McBain, 1996; Ali & Thomson, 1998; Lien *et al.* 2002). Mean 'sag' ratio in O-LM cells (–200 pA, 500 ms hyperpolarizing current injection) was 0.79 ± 0.02 ($n = 10$). During intrasomatic current injection trilaminar cells discharged in clusters of short-duration action potentials (Table 1, Fig. 3*C*). Afterhyperpolarization (AHP) decayed significantly faster in trilaminar cells than in O-LM cells (Table 1, Fig. 3*C*). In response to depolarizing current injection (up to 600 pA), the O-LM cells showed significantly lower frequency discharges than trilaminar cells (Table 1). Mean initial and steady state firing frequencies were 130.0 ± 19.1 Hz and 70.0 ± 17.2 ms in O-LM ($n = 15$) and 179.3 ± 26.6 Hz and 110.0 ± 13.1 Hz in trilaminar cells ($n = 8$, $P < 0.05$ for both initial and steady state firing frequency). However, these cells demonstrated a similar degree of action potential accommodation to corresponding current pulse (the ratio of the steady state firing frequency to the initial frequency was 0.54% in O-LM and 0.61% in trilaminar cells, $P > 0.05$, Fig. 3*D* and *E*).

Concomitant patch-clamp and extracellular field potential recordings were used to study recruitment of these two types of interneurones in the emergent γ oscillations. During kainate-evoked gamma frequency activity both classes of interneurones with horizontal dendrites in stratum oriens (Fig. 2) received a sustained barrage of gamma frequency compound EPSCs (V_{hold} –70 mV) that were temporally correlated with

the antiphasic extracellular field oscillation (Fig. 4*A* and *B*).

A key difference, however, was observed in the firing properties of the two interneurone types. When analysing the firing pattern of cells it became apparent that individual O-LM interneurones did not fire action potentials on every γ cycle (Fig. 4*Cii*). O-LM cells instead discharged at theta frequency during the gamma oscillations. The average firing probability of O-LM interneurones during a cycle was $25.8 \pm 4.3\%$ and the mean firing frequency was in the theta frequency range (Table 1). While the power spectrum of the field oscillatory activity showed a peak in the gamma frequency range, the power spectrum of current clamp recording in O-LM interneurones demonstrated a clear peak at the theta frequencies following kainate ejection (Fig. 4*Ciii* and *iv*). Remarkably O-LM cells discharged with theta frequency not only at resting membrane potential but also at more depolarized level (mean membrane potential -49.7 ± 1.0 mV, $n = 4$) close to threshold of AP firing (Fig. 4*Dii*), with the average firing probability during a cycle of $28.4 \pm 5.6\%$ ($n = 4$) and a mean frequency of 9.1 ± 2.3 Hz ($n = 4$) suggesting that the observed firing properties during the gamma oscillations in fact reflect an actual cellular specificity of these cells. In contrast, trilaminar cells discharged on every cycle of the gamma frequency oscillation (Fig. 4*Eii*). Moreover, the latter showed a propensity to fire spike doublets (mean AP interval 5.73 ± 0.09 ms, $n = 8$). The power spectrum of current clamp recordings in trilaminar cells demonstrated a peak at the gamma frequency range (Fig. 4*Eiii–iv*).

A high frequency synaptic oscillatory component in horizontal interneurones

During gamma activity both O-LM and trilaminar interneurones show a dramatic increase in synaptic activity which is temporally coherent with concomitant extracellular recordings (Fig. 5*A* and *B*). Pooled power spectra exhibited a prominent peak in the gamma frequency range (32.9 ± 2.1 Hz in O-LM, $n = 6$ and 31.4 ± 2.2 Hz in trilaminar cells, $n = 6$, $P > 0.05$, Fig. 5*C* and *D*). The peak power of EPSC recordings in trilaminar cells was significantly larger than in O-LM cells (Table 2, Fig. 5*D*). The majority of EPSCs in both cell classes were clearly multiquantal, comprising clusters of high-frequency rhythmic events, which were separated by regular intervals of aperiodically occurring EPSCs. Simultaneous extracellular and patch-clamp recordings during gamma oscillations showed that such clusters of EPSCs in the O-LM interneurones were temporally correlated with the extracellularly recorded population activity (Fig. 5*Ai–ii*). Likewise, rhythmic, but significantly larger amplitude EPSCs were observed in trilaminar cells (Fig. 5*Bii*; note change in scale). When band-pass filtering epochs of compound EPSCs between 200 and 500 Hz the high-frequency oscillatory component of synaptic activity was dramatically accentuated (Fig. 5*Aiii* and *E*; and Fig. 5*Biii* and *F*). Such 'incremental' bursts of EPSCs occurred in all studied O-LM ($n = 15$) and trilaminar ($n = 8$) interneurones and further analysis of inter-event intervals revealed a similar periodicity in O-LM and trilaminar cells (Table 2, Fig. 5*G* and *H*), suggesting a common source of excitatory input.

EPSC/P properties distinguish O-LM and trilaminar interneurones

O-LM and trilaminar cells showed clear differences in the amplitude and kinetics of spontaneous EPSPs (sEPSP) (Table 2, Fig. 6*A*). Differences in EPSPs are also reflected in postsynaptic current recordings from these two classes of interneurones. As revealed by the voltage clamp recordings, the mean amplitude of spontaneous EPSCs (sEPSCs) in O-LM cells was significantly smaller than in trilaminar interneurones (Table 2, Fig. 6*B* and *C*). Likewise, the kinetics of synaptic events in both interneurone types were markedly different. The average 10–90% rise time and decay time constant of sEPSC in O-LM cells were significantly slower than in trilaminar interneurones (Table 2, Fig. 6*B* and *C*). The properties of spontaneous PSCs (amplitude, frequency) in both cell classes did not change significantly in the presence of bicuculline, a $GABA_A$ receptor antagonist (20 μM, $n = 4$), but these currents were completely blocked by additional application of an AMPA/kainate receptor antagonist, 1,2,3,4-tetrahydro-6-nitro-2,3-dioxo-benzo[f]quinoxaline-7-sulfonamide (NBQX; 10 μM, $n = 4$, data not shown) suggesting their excitatory nature. Interestingly, the differences in the kinetic properties of sEPSCs between the two interneurone types were also maintained during gamma frequency oscillations (Fig. 6*D* and *E*). The individual components of kainate-evoked compound EPSCs (eEPSCs) in O-LM cells were again significantly smaller than in trilaminar cells (Table 2, Fig. 6*D* and *E*). The mean 10–90% rise time and decay time constant of averaged eEPSCs in O-LM interneurones were slower than in trilaminar cells (Table 2, Fig. 6*D* and *E*, $P < 10^{-8}$, Kolmogorov-Smirnov statistics).

Comparisons with other types of fast spiking interneurones and pyramidal cells

Fast spiking perisomatic interneurones with a typical basket cell axonal arborization in the stratum pyramidale (Fig. 7*A*), have a mean resting membrane potential, input resistance, membrane time constant and action potential half-duration not significantly different from those in trilaminar cells (Table 1). Single action potentials

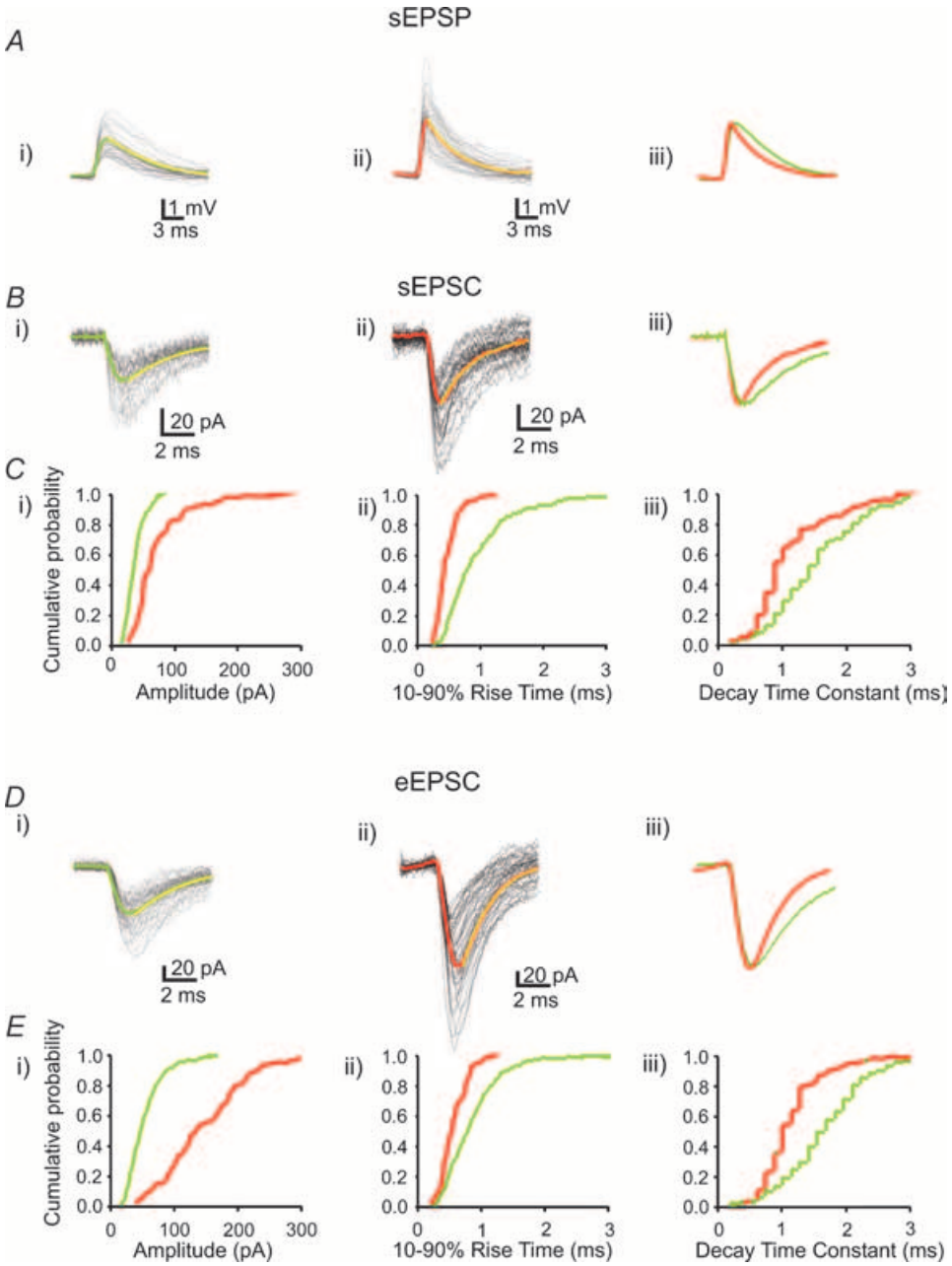

Figure 6. Comparison of EPSC/P kinetics in O-LM and trilaminar interneurones
A, O-LM cells (*i*) exhibit significantly smaller and slower spontaneous excitatory postsynaptic potentials (sEPSP) than trilaminar cells (*ii*), which are more clearly visible in superimposed and normalized traces (*iii*). *Ai–ii*, 40 individual traces are black and superimposed averaged potentials are green in O-LM and red in trilaminar cells. Decay of the averaged EPSPs in both classes of interneurones is well fitted by a single exponential function (yellow). *B*, differences in the properties of sEPSP in two types of interneurone are also reflected in postsynaptic current recordings. The averaged traces of spontaneous EPSCs (sEPSC, aligned from 40 individual traces) from an O-LM (*i*, green) and a trilaminar (*ii*, red) cell show clear differences in their amplitude, rise time and decay time constants, with kinetic differences being more accentuated in superimposed averages which have been normalized for amplitude (*iii*). *C*, cumulative probability plots (evaluated by 40 events from each individual cell) show marked differences in sEPSC kinetics between O-LM ($n = 8$) and trilaminar ($n = 6$) cells. Trilaminar interneurones had sEPSCs with larger amplitude (*i*, red, mean amplitude 72.3 ± 4.4 pA), faster rise time (*ii*, red, mean 10–90% rise time 0.48 ± 0.02 ms) and decay time constant (*iii*, red, mean decay time constant 1.65 ± 0.09 ms) compared with those recorded in O-LM cells (*i–iii*, green, 37.5 ± 1.2 pA, 0.84 ± 0.10 ms and 2.58 ± 0.09 ms, respectively). Kolmogorov-Smirnov statistics reveal a high level of statistical significance ($P < 10^{-7}$) for all parameters measured. *D*, suggesting a similar dendritic source, synaptic events with comparable kinetics were also found during kainate-evoked network oscillations in both O-LM (*i*) and trilaminar (*ii*) cells, with the larger amplitude of events being indicative of a

were followed by AHP which were longer though not significantly different from those in trilaminar cells (Table 1). These cells showed a low degree of spike frequency adaptation (Fig. 7*A*). During kainate-evoked oscillation these cells showed gamma frequency EPSCs (V_{hold} –70 mV) that were temporally correlated with the antiphasic extracellular field oscillation (Fig. 7*B*). In the current clamp mode, 4 of 6 studied perisomatic interneurones discharged with doublets of action potentials, which occurred irregularly (on every 1–5 field gamma cycles) and were interrupted by single action potentials during the gamma activity. Mean inter-doublet interval was 8.2 ± 0.2 ms ($n = 4$), significantly longer then those in trilaminar cells ($P < 0.05$). This doublet interval corresponded approximately to twice the interval between components of the compound EPSC invading these cells (4.22 ± 0.21 ms, Table 2). The remaining two cells generated exclusively single action potentials on every gamma cycle. Both, single spikes and doublets of action potentials were phase locked to the field (Fig. 7*D*).

The other class of fast spiking cells, bistratifed interneurones have axonal arborization in two (str. oriens and str. radiatum) layers (Fig. 8*A*). The intrinsic membrane properties in three cells were not significantly different from those in basket and trilaminar interneurones (Table 1). Single APs were followed by AHPs with significantly longer decay time constants (and half-duration) as those in trilaminar cells (Table 1). The EPSCs in recorded bistratified cells were also temporally correlated with the field potential oscillations (Fig. 8*B*). In current clamp mode these cells discharged on every gamma cycle. However, in contrast to the perisomatic interneurones, they generated exclusively a single action potential on every gamma cycle (Fig. 8*D*).

Perisomatic interneurones, similar to trilaminar cells, showed fast kinetics of sEPSCs/Ps and eEPSCs (Table 2 and Fig. 7*C*). Fast kinetic properties of sEPSCs/Ps and eEPSCs were also exhibited by three of the studied bistratified cells (Table 2 and Fig. 8*C*). Interestingly, although recorded perisomatic and bistratified interneurones showed similar compound EPSCs during the gamma activity (Figs 7*Bii* and 8*Bii*), in contrast to the horizontal cells, they exhibited a significantly longer inter-event intervals (Figs 7*Ciii* and 8*Ciii*, and Table 2). Pooled power spectra of compound EPSCs in these two types of cells also exhibited a prominent peak in the gamma frequency range (Table 2). The peak power of EPSC recordings in basket and bistratified cells were similar (Table 2, data not shown) and not significantly different from those in trilaminar cells.

Prominent differences were apparent when comparing the kinetic properties of EPSCs/Ps in CA3 pyramidal neurones with those in interneurones (Fig. 9*C* and *D*). In general, averaged pyramidal cell EPSCs had markedly slower time courses than those of interneurones (Table 2).

Action potential firing probability of pyramidal cells during a gamma cycle was low ($11.2 \pm 1.9\%$ with the mean firing frequency of 3.5 ± 0.6 Hz, $n = 9$; Table 1 and Fig. 9*E*), thus corroborating earlier *in vivo* (Bragin *et al.* 1995) and *in vitro* (Fisahn *et al.* 1998) observations, showing that pyramidal neurones do not fire action potentials on every cycle of γ activity.

Discussion

Using a pharmacological gamma-induction protocol to study oscillations in submerged slices, we have provided clear evidence that hippocampal interneurones exhibit different functional roles in the generation of hippocampal network oscillations. In terms of output the two extremes of behaviour were shown by O-LM cells, firing at theta frequencies (every 4–5 field gamma periods) and trilaminar cells (firing double spikes on every field gamma period). Between these two output patterns perisomatic targeting basket cells fired single action potentials, with occasional doublets, on each gamma period and bistratified cells invariably fired only once per period. Each of these cell types received similar, compound EPSC inputs at gamma frequencies during the field rhythm. A number of factors as we will argue below may account for the large range of output profiles seen in these different types of interneurones.

EPSC/P properties of the interneurones in the oscillatory network

Our data confirm findings showing that the properties of excitatory events discriminate hippocampal principal

greater degree of response summation. eEPSCs ($n = 40$ for each cell type, black) are aligned for averaging and calculating kinetic parameters of synaptic currents. Decay of the averaged eEPSC (green – O-LM, red – trilaminar) is well fitted by a single exponential function (yellow). *iii*, superimposed and normalized traces. *E*, group data showing corresponding cumulative probability plots (evaluated by 40 events from each individual cell) of the distribution of EPSC amplitude (*i*, mean -150.2 ± 8.9 pA), 10–90% rise time (*ii*, mean -0.53 ± 0.05 ms) and decay time constants (*iii*, mean -1.40 ± 0.23 ms) reveal that EPSCs in trilaminar cells (red, $n = 6$) show comparable differences to those observed at equivalent synapses onto O-LM interneurones (green, $n = 8$, mean -54.3 ± 1.7 pA, 0.84 ± 0.09 ms and 2.52 ± 0.20 ms, respectively). The differences in the kinetic parameters were significant ($P < 10^{-8}$, Kolmogorov-Smirnov statistics).

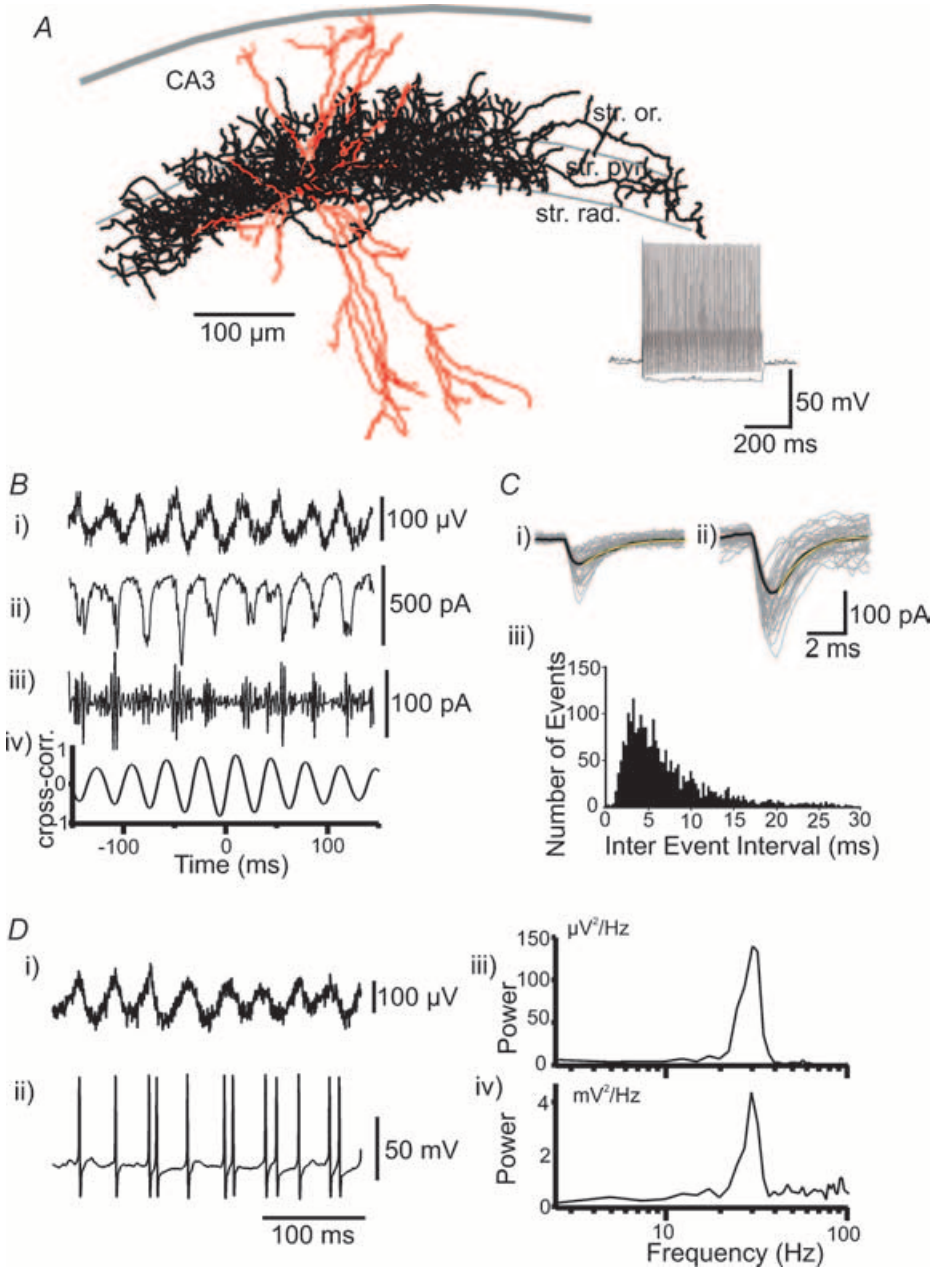

Figure 7. Electrophysiological and morphological characterization of perisomatic PV-positive cells
A, Neurolucida reconstruction of the biocytin-filled PV-positive basket cell. The soma and radial dendrites are drawn in red, whereas the axon is in black. The axonal branches from the basket cells are mainly restricted to stratum pyramidale. Hippocampal layers are depicted schematically. CA3, CA3 area; str. or., stratum oriens; str. pyr., stratum pyramidale; str. rad., stratum radiatum. The inset shows a typical response of these cells during intrasomatic depolarizing (600 nA) and hyperpolarizing (–200 pA) current injection. Note a fast firing in basket cell in response to depolarizing current injection. *B*, a whole-cell voltage clamp (*ii*) recording during kainate-induced epochs of gamma oscillations (V_m –70 mV) is phase related (*iv*) to concomitant recorded field potential (*i*). In band-pass filtered (200–500 Hz; *iii*) trace, basket cell shows a high-frequency oscillatory component. *C*, sEPSCs (*i*) and eEPSCs (*ii*, $n = 40$ for each current, grey) are aligned for averaging and calculating kinetic parameters of EPSCs. Decay of the averaged EPSC (black) is well fitted by a single exponential function (yellow). *iii*, histogram of inter-event intervals from unfiltered patch clamp recordings in basket cells. *D*, current clamp recording from perisomatic neurone (membrane potentials –60 mV) shows that this cell discharged with single spikes interrupted by irregularly occurring doublets of action potentials (*ii*), phase locked to the field gamma activity (*i*). *Diii* and *iv*, power spectra illustrating oscillatory activity at the gamma frequency range in perisomatic interneurone (*iv*) during the field gamma frequency oscillations (*iii*).

cells from inhibitory neurones (Miles, 1990; Jonas *et al.* 1993; Geiger *et al.* 1997; Toth *et al.* 2000). It appears that excitatory synapses onto interneurones not only tend to have a larger number of AMPA receptors (Nusser *et al.* 1998), thereby increasing the quantal amplitude, but the postsynaptic receptors also appear to have a different molecular composition (Geiger *et al.* 1995), which, in turn, endows them with faster kinetics

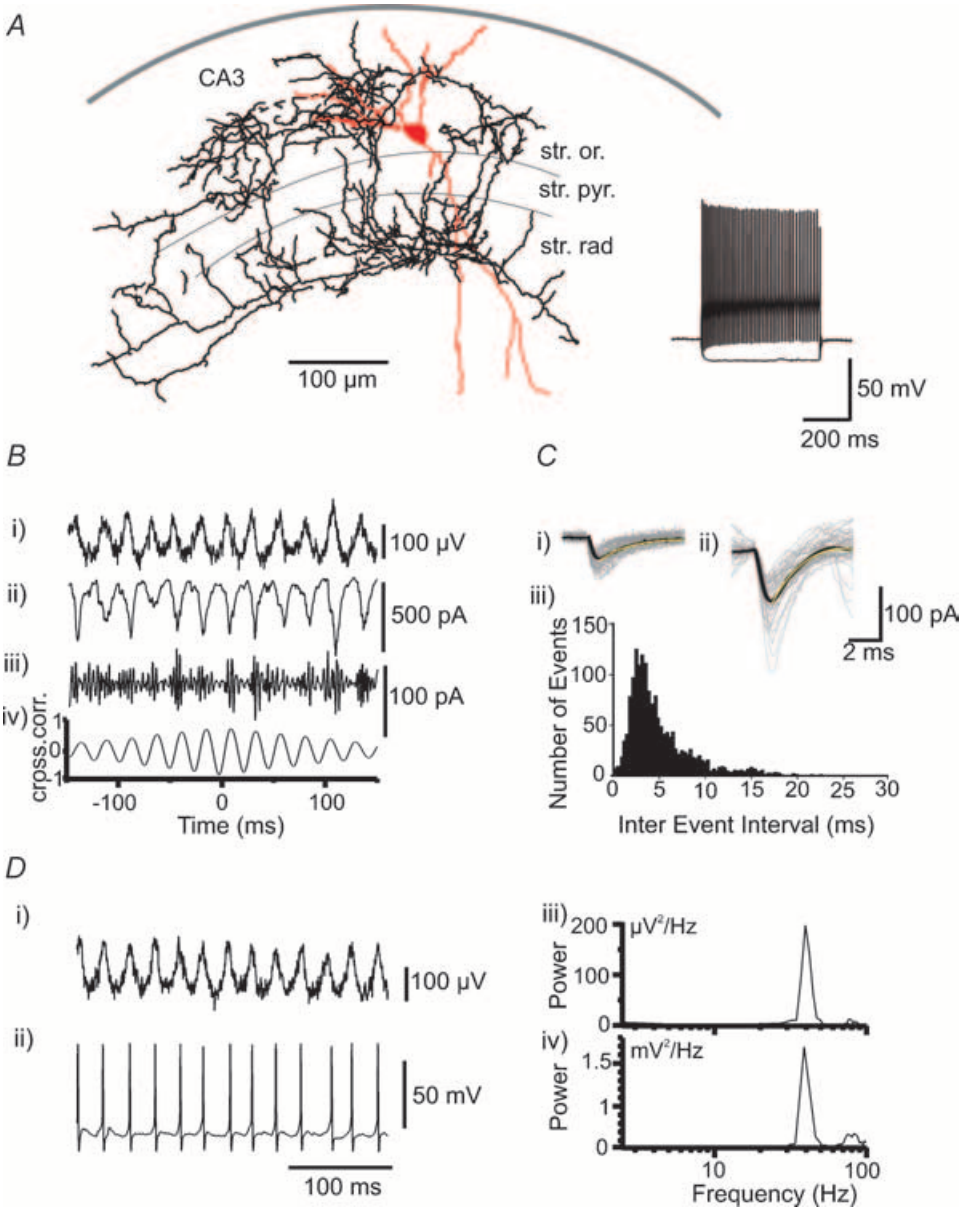

Figure 8. Electrophysiological and morphological properties of the bistratified interneuons
A, Neurolucida reconstruction of the bistratified cell. The axon (black) of the interneurone (soma and dendrites in red) is largely restricted to the str. oriens and radiatum. Note the sparing by axon of str. pyramidale, and the radially extending dendritic branches. CA3, CA3 area; str. or., stratum oriens; str. pyr., stratum pyramidale; str. rad., stratum radiatum. Inset, response to hyper- (–200 pA) and depolarizing (600 pA) current injection. Note the fast firing character of this cell. *B*, typical example of concomitant extracellular field (*i*) and voltage clamp recordings (*ii*) in a bistratified cell following induction of oscillatory activity and their cross-correlation (*iv*). In band pass filtered (200–500 Hz; *iii*) trace the bistratified cell also shows a high-frequency oscillatory component. *C*, superimposed single sEPSC (*i*) and eEPSC (*ii*, $n = 40$ for each synaptic currents, grey) and corresponding averaged synaptic currents (black) in a bistratified cell. Decay of the averaged currents is well fitted by a single exponential function (yellow). *iii*, histogram of inter-event intervals from unfiltered patch clamp recordings in bistratified cells. *D*, current clamp recording (at –60 mV) from the same cell as in *B* and *C* demonstrates single action potentials (*ii*) on every field gamma cycle (*i*). Corresponding power spectra from the field potential (*iii*) and current clamp (*iv*) recordings show the clear peaks at gamma frequency.

(Geiger *et al.* 1997). Hence temporal summation of EPSPs in interneurones is restricted to a relatively narrow time window and, accordingly, both computational simulations and experimental data suggest that interneurones act as coincidence detectors (Konig *et al.* 1996; Galarreta & Hestrin, 2001), whereas pyramidal cells are more suitable to integrate the overall level of postsynaptic activity.

The kinetic properties of excitatory events in stratum pyramidale interneurones have profound effects on network activity associated with changes in interneurone firing patterns (Fuchs *et al.* 2001). Here we provide evidence that different classes of str. oriens interneurones with distinct axonal ramification patterns and efferent target profiles show clear differences in both amplitude and kinetics of EPSCs/Ps. As suggested above, it is possible to explain these data solely with differences in the number and properties of AMPA/kainate receptors. However, in view of the presumably inadequate voltage clamp of remote dendritic sites, other factors may also affect the magnitude and kinetics of excitatory events, amongst them passive membrane properties, voltage-gated dendritic conductances and the electrotonic remoteness of synaptic junctions.

During kainate-evoked oscillatory activity the interneurones studied here receive gamma-frequency compound EPSPs which are temporally correlated with extracellular population activity. In view of the slice being de-afferented, it is likely that the action potential-dependent excitatory events are mediated by local excitatory feedback loops which originate in neighbouring pyramidal neurones. Although the latter fire only sporadically during gamma activity, interneurones, for three reasons, may receive a rhythmic barrage of gamma frequency EPSPs. First, in the active network, in view of their large numbers, at least several pyramidal cells are likely to fire on any given oscillatory cycle. Second, due to the convergence of numerous pyramidal cell recurrent axons onto a single postsynaptic interneurone it follows that each interneurone is also likely to receive a small number of unitary excitatory inputs on each successive gamma wave. Third, activity in pyramidal cell axons could orthodromically excite interneurones, without pyramidal cell somata necessarily firing (Traub *et al.* 2003).

Despite the range of interneuronal outputs seen during gamma activity (O-LM theta frequency output up to

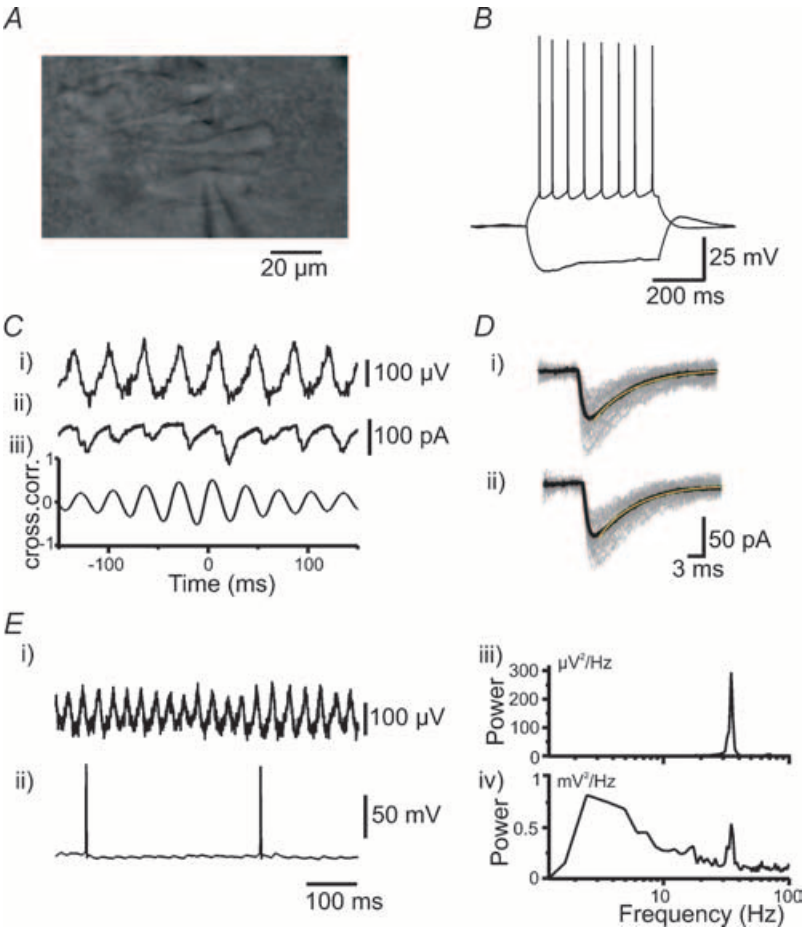

Figure 9. Properties of the area CA3 pyramidal cells
A, IR videomicroscopy image of the pyramidal cell in str. pyramidale. Alveus is on the right side. *B*, response of the pyramidal cell to hyperpolarizing (of –200 pA) and depolarizing (200 pA) current injection. Note regular firing of the pyramidal cell. *C*, during kainate-evoked network activity the pyramidal cells show gamma frequency EPSCs (*ii*, V_{hold} –70 mV) that were temporally correlated with the extracellular field oscillation (*i* and *iii*). *D*, kinetics of postsynaptic currents (both sEPSC and eEPSC) were significantly slower in pyramidal cells than those in interneurones (40 individual traces for both sEPSC (*i*) and eEPSC (*ii*) are in grey and the average synaptic currents in black). In these cells the decay of the averaged currents were also well fitted by a single exponential function (*i* and *ii*, yellow). *E*, concomitant field potential (*i*) and current clamp (*ii*) recordings in a pyramidal cell during the gamma activity showing the low frequency discharges in this cell. *iii* and *iv*, corresponding power spectra illustrating the low frequency peak in the pyramidal cell (*iv*) during the gamma peak in the field recording (*iii*).

trilaminar neuronal doublets), little difference was seen in the frequency of EPSCs within the phasic compound excitatory events. The amplitudes of excitatory drive were considerably larger in doublet-firing trilaminar cells than O-LM cells, suggesting the intensity of synaptic drive may play a role in generating such different outputs. However, similar phasic drives were seen in basket and bistratified cells compared with trilaminar cells but these cells rarely, or never, fired action potential doublets. Marked differences in EPSC kinetics were also seen in cells at the ends of the output range (theta *versus* gamma doublet). Slower kinetics in O-LM cells may be expected to increase temporal summation of individual components of the compound EPSC during gamma oscillations but this did not result in larger phasic drive. In summary, though differences in amplitude and kinetics of EPSCs existed between the different interneurone subtypes no clear pattern sufficient to explain the range of output profiles could be found in EPSCs alone.

Intrinsic properties of interneurones with respect to firing patterns

The most striking finding in terms of interneurone output was that O-LM cells generated a robust theta frequency output whereas the other interneurones fired action potentials (singly or as doublets) at gamma frequencies. Near firing threshold O-LM cells show prominent membrane potential oscillations in the theta frequency range (T. Gloveli, M. A. Whittington, E. H. Buhl, unpublished observations; Maccaferri & McBain, 1996), whereas hippocampal fast-spiking cells preferentially resonate in the gamma range (Pike *et al.* 2000), thus endowing both types of cell with a greater propensity to discharge in a different frequency band. In addition, O-LM cells had a longer membrane time constant than the gamma-preferring interneurones and a considerably longer AHP. Changes in AHP profiles in interneurones have been shown to have dramatic effects on firing patterns (e.g. see Lau *et al.* 2000; Savic *et al.* 2001). The decay time constant of AHP in O-LM cells was some 5- to 10-fold slower than in interneurones generating gamma frequency outputs. In contrast trilaminar cells had the most rapid AHP (decay time constant less than 0.5 ms). This, coupled with the larger phasic synaptic excitation may, in part, explain the marked output profile differences of these two cells for a given temporal pattern of phasic input.

Different roles for interneurones during network oscillations

In vivo (Csicsvari *et al.* 2003), *in vitro* (Fisahn *et al.* 1998) and computational models of pharmacologically evoked persistent gamma activity (Traub *et al.* 2000) have revealed a critical involvement of phasic excitatory input onto interneurones. In our model of locally generated gamma oscillations the pattern of excitatory input was broadly similar in each interneurone class. The differences in output characteristics appeared to correspond mainly to the intrinsic temporal properties of these interneuronal membranes. The range of output profiles seen was accompanied by specific axonal arborization and terminal field profiles in the different cell types. Both bistratified and basket cells generated a predominantly gamma frequency output and targeted proximal dendritic and perisomatic pyramidal neuronal compartments. These anatomical and electrophysiological properties make these neurones ideally suited for generating local gamma rhythms. Given the same network stimulus O-LM cells generated a theta frequency output and targeted basal and distal apical dendritic fields. During field gamma oscillations a more prominent theta frequency inhibitory input to distal apical dendrites has been reported (Gillies *et al.* 2002). At the local network level it therefore appears that specific interneurones generating gamma frequency outputs present this output preferentially to perisomatic and proximal dendritic compartments. Interneurones generating theta frequency outputs target more distal dendritic compartments (certainly in the apical arbour). *In vivo* oscillatory activity in the hippocampus frequently takes the form of a gamma rhythm nested in a theta rhythm (Penttonen *et al.* 1998). This phenomenon may reflect a division of labour amongst interneurones whereby the two frequencies are generated by two distinct subclasses of interneurone and projected to different compartments of principal cells.

The most powerful interneuronal output seen during local gamma oscillations was associated with trilaminar interneurones. These cells generated highly regular fixed, short latency spike doublets. Due to the axonal arborization profile of these interneurones, this output would be targeted not only onto somatic and dendritic – though not apical distal dendritic – compartments of local pyramidal cells, but also onto more distal sites. Axon collaterals were seen projecting all the way along area CA1 and into the subiculum. Thus, via these cells, gamma rhythms generated locally in area CA3 could be efficiently broadcast to distal sites 'downstream' in the classical hippocampal processing pathway.

We conclude that anatomical, intrinsic electrophysiological, and to some extent synaptic, properties combine to govern the role of different interneurone subclasses during a local hippocampal field oscillation. Different interneurones are associated with different network frequencies, different compartmental presentation of inhibitory inputs to principal cells and different local and distal communication of the interneuronally mediated rhythm. Given the very broad array of interneurone subtypes in the hippocampus alone,

the small sample presented here suggests that each interneurone subtype may play a specific, and perhaps unique, role in network activity.

References

Ali BA & Thomson AM (1998). Facilitating pyramid to horizontal oriens–alveus interneurone inputs: dual intracellular recordings in slices of rat hippocampus. *J Physiol* **507**, 185–199.

Bragin A, Jando G, Nadasdy Z, Hetke J, Wise K & Buzsaki G (1995). Gamma (40–100 Hz) oscillation in the hippocampus of the behaving rat. *J Neurosci* **15**, 47–60.

Buhl EH, Halasy K & Somogyi P (1994). Diverse sources of hippocampal unitary inhibitory postsynaptic potentials and the number of synaptic release sites. *Nature* **368**, 823–828.

Buzsaki G, Leung LW & Vanderwolf CH (1983). Cellular bases of hippocampal EEG in the behaving rat. *Brain Res* **287**, 139–171.

Csicsvari J, Jamieson B, Wise KD & Buzsaki G (2003). Mechanisms of gamma oscillations in the hippocampus of the behaving rat. *Neuron* **37**, 311–322.

Dodt HU & Zieglgansberger W (1990). Visualizing unstained neurones in living brain slices by infrared DIC-videomicroscopy. *Brain Res* **537**, 333–336.

Dodt HU & Zieglgansberger W (1994). Infrared videomicroscopy: a new look at neuronal structure and function. *Trends Neurosci* **17**, 453–458.

Fisahn A, Pike FG, Buhl EH & Paulsen O (1998). Cholinergic induction of network oscillations at 40 Hz in the hippocampus in vitro. *Nature* **394**, 186–189.

Freund TF & Buzsaki G (1996). Interneurones of the hippocampus. *Hippocampus* **6**, 347–470.

Fries P, Reynolds JH, Rorie AE & Desimone R (2001). Modulation of oscillatory neuronal synchronization by selective visual attention. *Science* **291**, 1560–1563.

Fuchs EC, Doheny H, Faulkner H, Caputi A, Traub RD, Bibbig A *et al.* (2001). Genetically altered AMPA-type glutamate receptor kinetics in interneurones disrupt long-range synchrony of gamma oscillation. *Proc Natl Acad Sci U S A* **98**, 3571–3576.

Galarreta M & Hestrin S (2001). Spike transmission and synchrony detection in networks of GABAergic interneurones. *Science* **292**, 2295–2299.

Geiger JR, Lubke J, Roth A, Frotscher M & Jonas P (1997). Submillisecond AMPA receptor-mediated signaling at a principal neuron-interneuron synapse. *Neuron* **18**, 1009–1023.

Geiger JR, Melcher T, Koh DS, Sakmann B, Seeburg PH, Jonas P *et al.* (1995). Relative abundance of subunit mRNAs determines gating and Ca^{2+} permeability of AMPA receptors in principal neurones and interneurones in rat CNS. *Neuron* **15**, 193–204.

Gillies MJ, Traub RD, LeBeau FEN, Davies CH, Gloveli T, Buhl EH *et al.* (2002). A model of atropine-resistant theta oscilations in rat hippocampal area CA1. *J Physiol* **543**, 779–793.

Gray CM, Konig P, Engel AK & Singer W (1989). Oscillatory responses in cat visual cortex exhibit inter-columnar synchronization which reflects global stimulus properties. *Nature* **338**, 334–337.

Gray CM & Singer W (1989). Stimulus-specific neuronal oscillations in orientation columns of cat visual cortex. *Proc Natl Acad Sci U S A* **86**, 1698–1702.

Hormuzdi SG, Pais I, LeBeau FE, Towers SK, Rozov A, Buhl EH *et al.* (2001). Impaired electrical signaling disrupts gamma frequency oscillations in connexin 36-deficient mice. *Neuron* **31**, 487–495.

Jonas P, Major G & Sakmann B (1993). Quantal components of unitary EPSCs at the mossy fibre synapse on CA3 pyramidal cells of rat hippocampus. *J Physiol* **472**, 615–663.

Jones MS & Barth DS (1997). Sensory-evoked high-frequency (gamma-band) oscillating potentials in somatosensory cortex of the unanesthetized rat. *Brain Res* **768**, 167–176.

Klausberger T, Magill PJ, Marton LF, Roberts JD, Cobden PM, Buzsaki G *et al.* (2003). Brain-state- and cell-type-specific firing of hippocampal interneurones in vivo. *Nature* **421**, 844–848.

Klausberger T, Marton LF, Baude A, Roberts JD, Magill PJ & Somogyi P (2004). Spike timing of dendrite-targeting bistratified cells during hippocampal network oscillations in vivo. *Nat Neurosci* **7**, 41–47.

Konig P, Engel AK & Singer W (1996). Integrator or coincidence detector? The role of the cortical neuron revisited. *Trends Neurosci* **19**, 130–137.

Lacaille JC & Williams S (1990). Membrane properties of interneurons in stratum oriens-alveus of the CA1 region of rat hippocampus in vitro. *Neuroscience* **36**, 349–359.

Lau D, Vega-Saenz de Miera EC, Contreras D, Ozaita A, Harvey M, Chow A *et al.* (2000). Impaired fast-spiking, suppressed cortical inhibition, and increased susceptibility to seizures in mice lacking Kv3.2 K^+ channel proteins. *J Neurosci* **20**, 9071–9085.

Lien CC, Martina M, Schultz JH, Ehmke H & Jonas P (2002). Gating, modulation and subunit composition of voltage-gated K^+ channels in dendritic inhibitory interneurones of rat hippocampus. *J Physiol* **538**, 405–419.

Maccaferri G & Lacaille JC (2003). Interneuron diversity series: Hippocampal interneuron classifications – making things as simple as possible, not simpler. *Trends Neurosci* **26**, 564–571.

Maccaferri G & McBain CJ (1996). The hyperpolarization-activated current (I_h) and its contribution to pacemaker activity in rat CA1 hippocampal stratum oriens–alveus interneurones. *J Physiol* **497**, 119–130.

Maccaferri G, Roberts JD, Szucs P, Cottingham CA & Somogyi P (2000). Cell surface domain specific postsynaptic currents evoked by identified GABAergic neurones in rat hippocampus in vitro. *J Physiol* **524**, 91–116.

McBain CJ & Fisahn A (2001). Interneurones unbound. *Nat Rev Neurosci* **2**, 11–23.

Meyer AH, Katona I, Blatow M, Rozov A & Monyer H (2002). In vivo labeling of parvalbumin-positive interneurons and analysis of electrical coupling in identified neurons. *J Neurosci* **22**, 7055–7064.

Miles R (1990). Synaptic excitation of inhibitory cells by single CA3 hippocampal pyramidal cells of the guinea-pig in vitro. *J Physiol* **428**, 61–77.

Morris RG, Garrud P, Rawlins JN & O'Keefe J (1982). Place navigation impaired in rats with hippocampal lesions. *Nature* **297**, 681–683.

Nusser Z, Lujan R, Laube G, Roberts JD, Molnar E & Somogyi P (1998). Cell type and pathway dependence of synaptic AMPA receptor number and variability in the hippocampus. *Neuron* **21**, 545–559.

Penttonen M, Kamondi A, Acsady L & Buzsaki G (1998). Gamma frequency oscillation in the hippocampus of the rat: intracellular analysis in vivo. *Eur J Neurosci* **10**, 718–728.

Pike FG, Goddard RS, Suckling JM, Ganter P, Kasthuri N & Paulsen O (2000). Distinct frequency preferences of different types of rat hippocampal neurones in response to oscillatory input currents. *J Physiol* **529**, 205–213.

Ritz R & Sejnowski TJ (1997). Synchronous oscillatory activity in sensory systems: new vistas on mechanisms. *Curr Opin Neurobiol* **7**, 536–546.

Savic N, Pedarzani P & Sciancalepore M (2001). Medium afterhyperpolarization and firing pattern modulation in interneurons of stratum radiatum in the CA3 hippocampal region. *J Neurophysiol* **85**, 1986–1997.

Sik A, Penttonen M, Ylinen A & Buzsaki G (1995). Hippocampal CA1 interneurones: an in vivo intracellular labeling study. *J Neurosci* **15**, 6651–6665.

Singer W & Gray CM (1995). Visual feature integration and the temporal correlation hypothesis. *Annu Rev Neurosci* **18**, 555–586.

Soltesz I & Deschenes M (1993). Low- and high-frequency membrane potential oscillations during theta activity in CA1 and CA3 pyramidal neurones of the rat hippocampus under ketamine-xylazine anesthesia. *J Neurophysiol* **70**, 97–116.

Spruston N, Lubke J & Frotscher M (1997). Interneurons in the stratum lucidum of the rat hippocampus: an anatomical and electrophysiological characterization. *J Comp Neurol* **385**, 427–440.

Toth K, Suares G, Lawrence JJ, Philips-Tansey E & McBain CJ (2000). Differential mechanisms of transmission at three types of mossy fiber synapse. *J Neurosci* **20**, 8279–8289.

Traub RD, Bibbig A, Fisahn A, LeBeau FE, Whittington MA & Buhl EH (2000). A model of gamma-frequency network oscillations induced in the rat CA3 region by carbachol in vitro. *Eur J Neurosci* **12**, 4093–4106.

Traub RD, Cunningham MO, Gloveli T, LeBeau FE, Bibbig A, Buhl EH *et al.* (2003). GABA-enhanced collective behavior in neuronal axons underlies persistent gamma-frequency oscillations. *Proc Natl Acad Sci U S A* **100**, 11047–11052.

Whittington MA, Traub RD & Jefferys JG (1995). Synchronized oscillations in interneuron networks driven by metabotropic glutamate receptor activation. *Nature* **373**, 612–615.

Zola-Morgan S & Squire LR (1993). Neuroanatomy of memory. *Annu Rev Neurosci* **16**, 547–563.

Acknowledgements

This study was supported by the SFB TR3/B5 to T.G., T.D. and U.H.; and the MRC, the Wellcome Trust, NIH/NIDS and EU grant to the late E.H.B. We thank Dr F. E. N. LeBeau for comments on the manuscript and D. Harrison for expert technical assistance.